Sequential Bond Energies of $Pt(CO)_x^+$ ($x = 1-4$) Determined by Collision-Induced Dissociation

Xiao-Guang Zhang and P. B. Armentrout*

Department of Chemistry, University of Utah, Salt Lake City, Utah 84112-0850

Received May 14, 2001

The sequential bond energies of $Pt(CO)_x^+$ ($x = 1-4$) are determined by collision-induced dissociation with Xe using guided-ion beam tandem mass spectrometry. Analysis of the kinetic energy dependent cross sections yields 0 K bond energies in eV (kJ/mol) of 2.20 ± 0.10 (212 ± 10), 2.00 ± 0.10 (193 ± 10), 1.02 ± 0.05 (98 ± 5), and 0.55 ± 0.05 (53 ± 5) for $(CO)_{x-1}Pt^+-CO$ with $x = 1-4$, respectively. These values are in reasonable agreement with results of density functional ab initio calculations in the literature. $D_0(Pt^+-Xe)$ is determined as 0.86 ± 0.30 eV (83 ± 29 kJ/mol) from analysis of the ligand exchange reaction with $PtCO^+$. The trend in these bond energies is compared with those of nickel and sodium carbonyl cations and discussed in terms of sdσ hybridization, electrostatic interactions, and ligand−ligand steric interactions.

Introduction

Transition metal carbonyls are fundamental building blocks for organometallic synthesis and important catalysts for industrial applications.[1] Fundamental studies designed to elucidate the mechanisms of such chemistry often point to unsaturated organometallic species as key intermediates, but there is little accurate information about the thermochemistry of such species. Some information comes from calorimetric measurements on stable precursors;[2] however, these data provide only average rather than individual bond energies. The individual bond dissociation energies (BDEs) can vary significantly with the degree of ligation around the central metal ion, reflecting variations in geometric and electronic structures.[3−19] A number of studies have been carried out in the gas phase to obtain sequential bond energies of cationic,[3−11,20−22] neutral,[23−27] and anionic[17,18,28] metal−carbonyl species. A versatile approach to determine accurate sequential bond energies for metal carbonyl systems is to generate individual $M(CO)_x^+$ or $M(CO)_x^-$ species in the gas phase and to use a mass spectrometer to monitor their energy-dependent decomposition induced by collisions with a neutral partner. The gas phase is an ideal arena for detailed study of the energetics of bond-making and bond-breaking processes of such reactive species because solvation effects are absent, the coordinately and electronically unsaturated ions can be isolated, and their intrinsic reactivity can be observed straightforwardly.

Although the first CO coordinative compounds ever made were carbonyl halides of Pt, by Schutzenberger in 1868−1870,[1] homoleptic platinum carbonyl complexes analogous to nickel tetracarbonyl have not been prepared. However, neutral, cationic, and anionic platinum carbonyl complexes have been characterized recently using matrix-isolation techniques coupled with density

(1) Cotton, F. A.; Wilkinson, G. *Advanced Inorganic Chemistry,* 5th ed.; John Wiley & Sons: New York, 1988. Crabtree, R. H. *The Organometallic Chemistry of the Transition Metals*, 2nd ed.; John Wiley & Sons: New York, 1994.
(2) Pilcher, G.; Carson, A. S. In *Energetics of Organometallic Species*; Simões, J. A. M., Ed.; Kluwer Academic: Dordrecht, 1992; pp 9 and 131.
(3) Schultz, R. H.; Crellin, K. C.; Armentrout, P. B. *J. Am. Chem. Soc.* **1991**, *113*, 8590.
(4) Khan, F. A.; Clemmer, D. E.; Schultz, R. H.; Armentrout, P. B. *J. Phys. Chem.* **1993**, *97*, 7978.
(5) Sievers, M. R.; Armentrout, P. B. *J. Phys. Chem.* **1993**, *99*, 8135.
(6) Goebel, S.; Haynes, C. L.; Khan, F. A.; Armentrout, P. B. *J. Am. Chem. Soc.* **1995**, *117*, 6994.
(7) Khan, F. A.; Steele, D. L.; Armentrout, P. B. *J. Phys. Chem.* **1995**, *99*, 7819.
(8) Meyer, F.; Chen, Y.-M.; Armentrout, P. B. *J. Am. Chem. Soc.* **1995**, *117*, 4071.
(9) Meyer, Y.-M.; Armentrout, P. B. *Mol. Phys.* **1996**, *88*, 187.
(10) Walter, D.; Sievers, M. R.; Armentrout, P. B. *J. Phys. Chem.* **1993**, *99*, 8135.
(11) Andersen, A.; Muntean, F.; Walter, D.; Rue, C.; Armentrout, P. B. *J. Phys. Chem. A* **2000**, *104*, 692.
(12) Ervin, K.; Loh, S. K.; Aristov, N.; Armentrout, P. B. *J. Phys. Chem.* **1983**, *87*, 3593.
(13) Aristov, N.; Armentrout, P. B. *J. Phys. Chem.* **1986**, *90*, 5135.
(14) Magnera, T. F.; David, D. E.; Michl, J. *J. Am. Chem. Soc.* **1989**, *111*, 4100.
(15) Magnera, T. F.; David, D. E.; Stulik, D.; Orth, R. G.; Jonkman, H. T.; Michl, J. *J. Am. Chem. Soc.* **1989**, *111*, 5036.
(16) Marinelli, P. J.; Squires, R. R. *J. Am. Chem. Soc.* **1989**, *111*, 4101.
(17) Sunderlin, L. S.; Wang, D.; Squires, R. R. *J. Am. Chem. Soc.* **1992**, *114*, 2788.
(18) Sunderlin, L. S.; Wang, D.; Squires, R. R. *J. Am. Chem. Soc.* **1993**, *115*, 12060.
(19) Liang, B.; Zhou, M.; Andrews, L. *J. Phys. Chem. A* **2000**, *104*, 3905.
(20) Dearden, D. V.; Hayashibara, K.; Beauchamp, J. L.; Kirchner, N. J.; van Koppen, P. A. M.; Bowers, M. T. *J. Am. Chem. Soc.* **1989**, *111*, 2401.
(21) Bidinosti, D. R.; McIntyre, N. S. *Can. J. Chem. Soc.* **1967**, *45*, 641.
(22) Winters, R. E.; Kiser, R. W. *Inorg. Chem.* **1964**, *3*, 699. Distefano, G. *J. Res. Natl. Bur. Stand., Sect. A* **1970**, *74*, 233.
(23) Ray, U.; Brandow, S. L.; Bandukwalla, G.; Venkataraman, B.; Zhang, Z.; Vernon, M. *J. Chem. Phys.* **1988**, *89*, 4092.
(24) McQuaid, M. J.; Morris, K.; Gole, J. L. *J. Am. Chem. Soc.* **1988**, *110*, 5280.
(25) Venkataraman, B.; Hou, H.; Zhang, H.; Chen, S.; Bandukwalla, G.; Vernon, M. *J. Chem. Phys.* **1990**, *92*, 5338.
(26) Rayner, D. M.; Ishikawa, Y.; Brown, C. E.; Hackett, P. A. *J. Chem. Phys.* **1991**, *94*, 5471.
(27) Fletcher, T. R.; Rosenfeld, R. N. *J. Am. Chem. Soc.* **1988**, *110*, 2097.
(28) Stevens, A. E.; Feigerle, C. S.; Lineberger, W. C. *J. Am. Chem. Soc.* **1982**, *104*, 5026.

10.1021/om010390d CCC: $20.00
Publication on Web 08/31/2001

functional theory (DFT).[19] The present study was undertaken primarily to provide accurate BDEs for $(CO)_{x-1}Pt^+-CO$ by use of low-energy collision-induced dissociation (CID).[12−16,29,30] Studies in our laboratory have demonstrated that guided ion beam tandem mass spectrometry can be used to obtain accurate sequential BDEs for $M(CO)_x^+$ systems where M = Ti,[9] V,[5] Cr,[4,30] Fe,[3] Co,[6] Ni,[7] Cu,[8] Ag,[8] Li,[10] Na,[10] K,[10] and Mg.[11] In the present work, we apply this technique to determine sequential BDEs at 0 K for $Pt(CO)_x^+$ ($x = 1-4$) by analysis of the kinetic energy dependence of the CID with Xe. Such studies aim to provide experimentally determined BDEs as a benchmark for comparison with theoretical models of structure and bonding of metal carbonyl cations.[19,31] This is also part of ongoing efforts in our laboratory to understand the periodic trends in sequential BDEs of metal carbonyl complexes.[3−11]

Experimental Section

General Procedures. The guided ion beam mass spectrometer on which these experiments were performed has been described in detail previously.[29,32] Briefly, $Pt(CO)_x^+$ ($x = 1-4$) ions are generated in a direct current discharge flow tube source (DC/FT) described below, extracted from the source, accelerated, and focused into a magnetic sector momentum analyzer for mass selection of primary ions. The mass-selected ions are then decelerated to a desired kinetic energy and focused into an octopole ion beam guide that uses radio frequency electric fields to trap the ions in the radial direction and ensure complete collection of reactant and product ions.[33,34] The octopole passes through a static gas cell with an effective length of 8.26 cm that contains Xe at a low pressure (usually less than ~0.3 mTorr) so that multiple ion−molecule collisions are improbable. The unreacted parent and product ions are confined radially in the guide until they drift to the end of the octopole, where they are extracted, focused, and passed through a quadrupole mass filter for mass analysis of products. Ions are subsequently detected with a secondary electron scintillation ion detector using standard pulse counting techniques. Reaction cross sections are calculated from product ion intensities relative to reactant ion intensities after correcting for background signals.[35] Uncertainties in absolute cross sections are estimated to be ±20%.

The kinetic energy of the ions is varied in the laboratory frame by scanning the dc bias on the octopole rods with respect to the potential of the ion source region. Laboratory (lab) ion energies are converted to energies in the center-of-mass frame (CM) by using the formula $E_{CM} = E_{lab}m/(m + M)$, where m and M are the neutral Xe and ionic reactant masses, respectively. Two effects broaden the cross section data: the kinetic energy distribution of the reactant ion and the thermal motion of the neutral reactant gas (Doppler broadening).[36] The absolute zero and the full width at half-maximum (fwhm) of the kinetic energy distribution of the reactant ions are determined using the octopole beam guide as a retarding potential analyzer, as described previously.[35] The distributions of ion energies, which are independent of energy, are nearly Gaussian and have a typical fwhm of 0.4−0.8 eV (lab) in these studies. Uncertainties in absolute energy scale are ±0.05 eV (lab).

Ion Source. $Pt(CO)_x^+$ ions are produced in a DC/FT source,[29] consisting of a cathode held at high negative voltage (0.7−1.0 kV) over which a flow of approximately 90% He and 10% Ar passes at a total pressure of 0.3−0.4 Torr and ambient temperature. In this work, the cathode is platinum foil attached to an iron holder. Ar^+ ions created in the discharge are accelerated toward the platinum cathode, thereby sputtering Pt^+. $Pt(CO)_x^+$ ions are produced through three-body condensation after CO is introduced into the flow tube 15 cm downstream of the discharge zone at a pressure of ~2 mTorr. $Pt(CO)_x^+$ ions are then swept down the flow tube and undergo $\sim 10^5$ thermalizing collisions with He and $\sim 10^4$ collisions with Ar before entering the guided ion beam apparatus. These collisions with the He/Ar flow gas stabilize and thermalize the ions both rotationally and vibrationally. We assume that these ions are in their ground electronic state and that the internal energy of these clusters is well described by a Maxwell−Boltzmann distribution of rotational and vibrational states corresponding to 300 K, the temperature of the flow tube. Previous studies from this laboratory have shown that these assumptions are consistent with the production of thermalized ions under similar conditions.[3−11,37−40] Further, we have demonstrated that Pt^+ ions are generated in their $^2D_{5/2}$ ground state under these conditions.[41] Therefore, it seems likely that $Pt(CO)_x^+$ ions created under such conditions should also be formed in doublet spin electronic states, the ground states for $x = 1-4$.[19] No obvious evidence for the population of excited electronic states is observed in this work, as described below.

Data Analysis. Several systematic effects influence the ability to derive accurate thermodynamic information from CID thresholds. These effects include (a) multiple collisions with Xe, (b) efficiency of the translational to internal energy transfer, (c) internal excitation of reactant ions that can contribute to the measured thresholds, and (d) the lifetime of the dissociation ions. Here, we account for these factors as follows.

First, our CID experiments were performed under predominantly single-collision conditions, as noted above. However, there is always a finite probability of a second collision while the ions go through the collision cell of Xe. Previous CID studies in our laboratory have shown that multiple collisions can strongly affect CID threshold behavior.[3,42,43] This pressure effect can be eliminated, following a procedure developed previously,[43] by linearly extrapolating cross sections measured at different pressures of Xe to zero-pressure, rigorously single-collision conditions. It is these linearly extrapolated cross sections that are analyzed for their thresholds.

In addition, the choice of collision partner can make a difference in the threshold excitation function.[3,10,12,32,44] For reasons described in detail previously,[12,32,44] we use Xe as the collision partner because it is heavy and polarizable, making the collision more long-lived and hence more efficient at transferring kinetic energy to internal energy of the reactant ions. Some verification of this efficiency comes from direct measurements of energy transfer in the CID of $Cr(CO)_6^+$ with

(29) Schultz, R. H.; Armentrout, P. B. *Int. J. Mass Spectrom. Ion Processess* **1991**, *107*, 29.
(30) Muntean, F.; Armentrout, P. B. *J. Chem. Phys.* **2001**, *115*, 1213.
(31) Bauschlicher, C. W., Jr.; Langhoff, S. R.; Partridge, H. In *Organometallic Ion Chemistry*; Freiser, B. S., Ed.; Kluwer: Dordrecht, 1996; p 47.
(32) Loh, S. K.; Hales, D. A.; Lian, L.; Armentrout, P. B. *J. Chem. Phys.* **1989**, *90*, 5466.
(33) Teloy, E.; Gerlich, D. *Chem. Phys.* **1974**, *4*, 417.
(34) Gerlich, D. *Adv. Chem. Phys.* **1992**, *82*, 1.
(35) Ervin, K. M.; Armentrout, P. B. *J. Chem. Phys.* **1985**, *83*, 166.
(36) Chantry, P. J. *J. Chem. Phys.* **1971**, *55*, 2746.
(37) Armentrout, P. B. *Int. J. Mass Spectrom.* **2000**, *200*, 219.
(38) Armentrout, P. B.; Kickel, B. L. In *Organometallic Ion Chemistry*; Freiser, B. S., Ed., Kluwer: Dordrecht, 1996; p 1.
(39) Armentrout, P. B. In *Topics in Organometallic Chemistry*; Brown, J. M., Hofmann, P., Eds.; Springer-Verlag: Berlin, 1999; Vol. 4-I, p 1.
(40) Rodgers, M. T.; Armentrout, P. B. *J. Phys. Chem. A* **1997**, *101*, 1238.
(41) Zhang, X.-G.; Liyanage, R.; Armentrout, P. B. *J. Am. Chem. Soc.* **2001**, *123*, 5563.
(42) Loh, S. K.; Lian, L.; Hales, D. A.; Armentrout, P. B. *J. Chem. Phys.* **1988**, *89*, 3378.
(43) Hales, D. A.; Lian, L.; Armentrout, P. B. *Int. J. Mass Spectrom.* **1990**, *102*, 269.
(44) Hales, D. A.; Armentrout, P. B. *J. Cluster Sci.* **1990**, *1*, 127.

Table 1. Vibrational Frequencies, Zero-Point Energy, Rotational Constants, and Internal Energy of $Pt(CO)_x^+$ and CO [a]

species	vibrational frequencies (cm^{-1})	zero-point energy (eV)	rotational constants (cm^{-1})	E_{int}(300 K) (eV)
CO[b]	2169.8	0.13	1.931	0.03
$Pt(CO)^+$	383.3(2), 492.1, 2262.2	0.22	0.104	0.05
$Pt(CO)_2^+$	76.9 (2), 336.7, 347.8 (2), 421.1, 504.7 (2), 2262.2, 2315.4	0.45	0.042	0.12
$Pt(CO)_3^+$	67.3, 79.4, 85.5, 246.2, 290.9, 317.6, 328.9, 336.1, 391.8, 403.5, 436.7, 494.8, 2243.1, 2245.2, 2286.1	0.64	0.083, 0.042, 0.028	0.19
$Pt(CO)_4^+$	46.9, 69.4, 83.7, 84.1(2), 272.5(2), 284.4(2), 288.3, 297.9, 327.8, 404.8, 418.1, 433.4(2), 492.6, 2212.5(2), 2217.0, 2252.9	0.84	0.039, 0.039, 0.021	0.27

[a] Degeneracies in parentheses. Except for CO, calculated using DFT theory at the B3LYP level with the LANL2DZ effective core potential for Pt and 6-311+G* basis set for C and O from Liang, Zhou, and Andrews, refs 19 and 57. [b] Huber, K. P.; Herzberg, G. *Constants of Diatomic Molecules*; Van Nostrand-Reinhold: New York, 1979.

Xe.[30] Experimental distributions of residual kinetic energies are found to extend to zero, the point of 100% energy deposition, indicating that the collisional energy transfer is not impulsive and consistent with transient complex formation.

The internal energy of the reactant ions can contribute to the energy needed to induce dissociation.[3,44−46] The flow tube ion source is designed to provide thermalized ions, such that excess vibrational and rotational excitation is unlikely.[3,4,7,29,46−49] However, the rotational and vibrational energy of thermalized ions must be considered in the analysis of the CID thresholds. The internal energy of the ions is best handled by explicitly considering the entire distribution of populated rovibrational states. The model used to reproduce the cross sections of products at zero pressure of Xe is given by eq 1,[30,37,46,50,]

$$\sigma(E) = \sigma_0 \sum g_i (E + E_i - E_0)^n / E \qquad (1)$$

where σ_0 is an energy-independent scaling factor, E is the relative kinetic energy of the reactants, E_0 is the threshold energy for formation of products in their ground rovibrational and electronic states, and n is an adjustable parameter. The sum considers contributions from rovibrational states of the reactant ions, denoted by i, having energies E_i and populations g_i, where $\sum g_i = 1$. We assume that the relative reactivity, as reflected by σ_0 and n, is the same for all rovibrational states. The Beyer−Swinehart algorithm is used to evaluate the density of the rovibrational states of the ions,[51−53] and then the relative populations g_i are calculated by the appropriate Maxwell−Boltzmann distribution at 300 K, the temperature of the flow tube. Details about our implementation of this equation are given elsewhere.[3,37] The various sets of vibrational frequencies and rotational constants used to determine E_i in this work are taken from DFT calculations for $Pt(CO)_x^+$ and are given in Table 1.[19] The electronic energy of the $Pt(CO)_x^+$ reactant is believed to be negligible, as noted above. We recently demonstrated that the cross section form given in eq 1 is consistent with direct measurements of the energy transferred in collisions between $Cr(CO)_6^+$ with Xe.[30] These results provide increased confidence in the use of eq 1 to fit experimental data to obtain accurate thermodynamic information from CID thresholds.[30,37,38,54]

We explicitly examined lifetime effects on the thresholds by considering whether all ions with energies in excess of the bond energy dissociate within the experimental time window, roughly 10^{-4} s (as determined by time-of-flight measurements).[30,35] Dissociation of ions is expected to become slower as the size of the complex increases, such that the apparent threshold observed for dissociation can shift to energies higher than the thermodynamic threshold. The lifetime effect is taken into account using Rice−Ramsperger−Kassel−Marcus (RRKM) theory[55] in the phase space limit (PSL) using equations developed by Rodgers, Ervin, and Armentrout.[54] Briefly, the transition state (TS) for dissociation is modeled by loosely interacting products such that both dissociating fragments are free to rotate. This PSL is appropriate for ion−molecule complexes because the TS for the reverse, barrierless association process is accurately described as lying at the top of the centrifugal barrier. In this study, the 2-D external rotations are treated adiabatically but with centrifugal effects included, consistent with the discussion of Waage and Rabinovitch.[56] The adiabatic 2-D rotational energy is treated using a statistical distribution with explicit summation over the possible values of the rotational quantum number, as described in detail elsewhere.[54] The vibrational frequencies of the reactants and transition states are taken from the DFT calculations of Andrews and co-workers and are listed in Table 1.[19,57] In this work, we find that lifetime effects are fairly small, 0.005 eV for $Pt(CO)_3^+$ and $Pt(CO)_4^+$ and negligible for $PtCO^+$ and $Pt(CO)_2^+$, well within our experimental errors.

Before comparison with the experimental data, eq 1 is convoluted with the kinetic energy distributions of the reactant ions and Xe at 300 K. The σ_0, n, and E_0 parameters are then optimized using a nonlinear least-squares analysis to give the best reproduction of the data.[35] Error limits for E_0 are calculated from the range of threshold values for different data sets over a range of acceptable n values, from a variation of ±25% for the vibrational frequencies, and from the absolute error in the energy scale.

Because the vibrational, rotational, and translational energy distributions of the reactants are explicitly included in our modeling, the E_0 thresholds obtained here correspond to 0 K

(45) Chupka, W. A. In *Ion−Molecule Reactions*; Franklin, J. L., Ed.; Plenum: New York, 1972; Vol. 1, p 33.
(46) Armentrout, P. B. In *Advances in Gas-Phase Ion Chemistry*; Adams, N. G., Babcock, L. M., Eds.; JAI: Greenwich, 1992; Vol. 1, p 83.
(47) Fisher, E. R.; Armentrout, P. B. *J. Chem. Phys.* **1991**, *94*, 1150.
(48) Dalleska, N. F.; Honma, K.; Armentrout, P. B. *J. Am. Chem. Soc.* **1993**, *115*, 12125.
(49) Dalleska, N. F.; Honma, K.; Sunderlin, L. S.; Armentrout, P. B. *J. Am. Chem. Soc.* **1994**, *116*, 3519.
(50) Chesnavich, W. J.; Bowers, M. T. *J. Phys. Chem.* **1979**, *83*, 900.
(51) Beyer, T.; Swinehart, D. F. *Commun. Assoc. Comput. Mach.* **1973**, *16*, 379.
(52) Stein, S. E.; Rabinovitch, B. S. *Chem. Phys. Lett.* **1977**, *49*, 183. *J. Chem. Phys.* **1977**, *53*, 2438.
(53) Gilbert, R. G.; Smith, S. C. *Theory of Unimolecular and Recombination Reactions*; Blackwell Scientific: Oxford, 1990.
(54) Rodgers, M. T.; Ervin, K. M.; Armentrout, P. B. *J. Chem. Phys.* **1997**, *106*, 4499.
(55) Marcus, R. A.; Rice, O. K. *J. Phys. Colloid Chem.* **1951**, *55*, 894. Marcus, R. A. *J. Chem. Phys.* **1952**, *20*, 359. Rosenstock, H. M.; Wallenstein, M. B.; Wahrhaftig, A. L.; Eyring, H. *Proc. Natl. Acad. Sci. U.S.A.* **1952**, *38*, 667.
(56) Waage, E. V.; Rabinovitch, B. S. *Chem. Rev.* **1970**, *70*, 377.
(57) Liang, B.; Andrews, L. Personal communication.

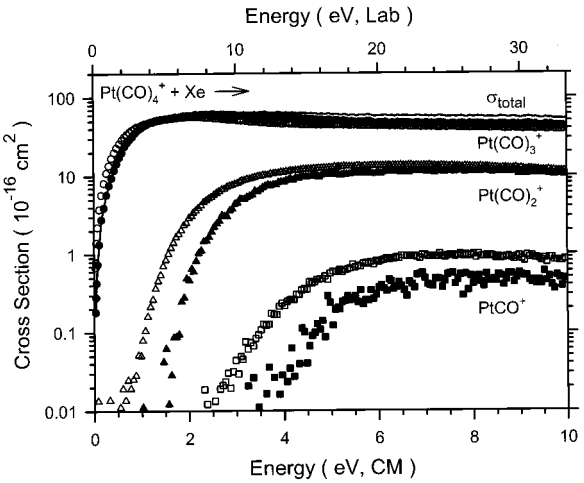

Figure 1. Cross sections for the reaction of $Pt(CO)_4^+$ with Xe as a function of kinetic energy in the center-of-mass frame (lower *x*-axis) and laboratory frame (upper *x*-axis). Sequential loss of CO ligands occurs to form $Pt(CO)_3^+$ (circles), $Pt(CO)_2^+$ (triangles), and $PtCO^+$ (squares). Open symbols were obtained at a pressure of 0.2 mTorr of Xe, whereas solid symbols are data extrapolated to zero pressure of Xe. The total dissociation cross section for loss of CO ligands at zero pressure of Xe is indicated by the solid line.

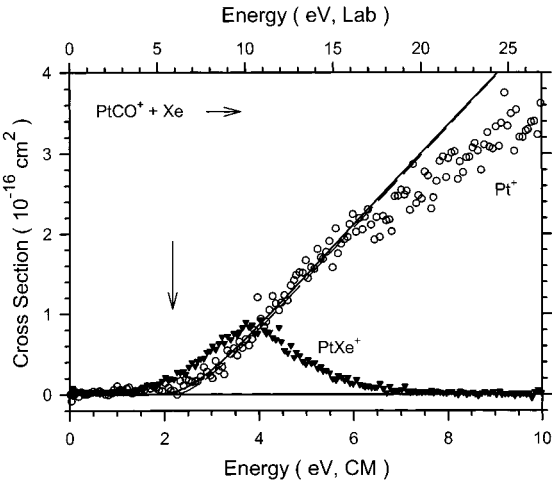

Figure 2. Zero pressure extrapolated cross sections for the reaction of $PtCO^+$ with Xe as a function of kinetic energy in the center-of-mass frame (lower *x*-axis) and laboratory frame (upper *x*-axis) to form Pt^+ (open circles) and $PtXe^+$ (solid inverted triangles). The dashed line is a model of the CID cross section that uses eq 1 with the parameters in Table 2 for 0 K reactants, and the solid line is the same model convoluted over the translational and rovibrational energy distributions of reactants. The vertical arrow indicates the 0 K threshold for loss of one CO ligand at 2.20 eV.

values. We take these thresholds to equal $D_0[(CO)_{x-1}Pt^+-CO]$, implicitly assuming that there are no activation energies in excess of the endothermicities for dissociation; that is, there are no reverse activation barriers. This assumption is reasonable for ion−molecule reactions because of the long-range ion-induced dipole and ion−dipole attractive potential.[37,38,46] In addition, theoretical considerations demonstrate that potential energy surfaces for heterolytic bond dissociations should have no intrinsic barriers.[58] An experimental study of the kinetic energy release distributions of the decomposition of $Mn(CO)_x^+$ complexes has demonstrated that this is a reasonable assumption for metal carbonyl species.[59] Curve crossings with surfaces of different spin could alter this situation, but no low lying excited electronic states of the $Pt(CO)_x^+$ species are expected and no evidence for such states is observed here.

Experimental Results

Collision-induced dissociation of $Pt(CO)_x^+$ species results in the sequential elimination of CO ligands. This is apparent in the data for $Pt(CO)_4^+$, shown in Figure 1, which is typical of the CID results for all the platinum carbonyl cations. There are no product ions observed with different numbers of C and O atoms. This observation is easily rationalized because the CO bond is substantially stronger than even the sum of the platinum−ligand bonds in $Pt(CO)_4^+$.

As shown in Figure 2, the interaction of $PtCO^+$ with Xe has Pt^+ as the major product, formed in the simple CID process, reaction 2.

$$Pt(CO)_x^+ + Xe \rightarrow Pt(CO)_{x-1}^+ + CO + Xe \qquad (2)$$

The Pt^+ cross section rises from an apparent threshold above 2 eV. The other product observed is $PtXe^+$, formed in the ligand exchange reaction 3.

$$PtCO^+ + Xe \rightarrow PtXe^+ + CO \qquad (3)$$

This product has an apparent threshold below that for the CID process, rises to a peak of about 0.9 Å at about 4 eV, and declines quickly at higher energies. The threshold for the ligand exchange process should represent the difference between the BDEs of Pt^+-CO and Pt^+-Xe.

Results for the interaction of $Pt(CO)_2^+$ with Xe are shown in Figure 3. The only product is $PtCO^+$, formed in the simple CID process, reaction 2. This cross section rises from an apparent threshold near 1.5 eV, lower than that for the CID process of $PtCO^+$, Figure 2, and then levels off above about 8 eV. No loss of two CO ligands from $Pt(CO)_2^+$ to form Pt^+ was observed, although this is probably because the experimental sensitivity is not sufficiently high.

The CID pattern of $Pt(CO)_3^+$, shown in Figure 4, is different from that of $PtCO^+$ and $Pt(CO)_2^+$. Here, the apparent threshold for the loss of a single CO is substantially lower, near 0.5 eV, and the cross section is larger. This cross section levels off at an energy close to the onset for formation of $PtCO^+$, showing that CO molecules are eliminated sequentially with increasing energy. No loss of three CO ligands from $Pt(CO)_3^+$ to form Pt^+ was observed, presumably a result of limited experimental sensitivity.

The CID pattern for $Pt(CO)_4^+$ is illustrated in Figures 1 and 5. The apparent threshold for the loss of a single CO is nearly zero, smaller than any of the other systems studied here. The $Pt(CO)_3^+$ cross section declines at the apparent onset of $Pt(CO)_2^+$ because of dissociation to the secondary dissociation product channel. The tertiary product channel is also observed at higher kinetic energies. The observed behavior is clearly a result of

(58) Armentrout, P. B.; Simons, J. *J. Am. Chem. Soc.* **1992**, *114*, 8627.
(59) Dearden, D. V.; Hayashibara, K.; Beauchamp, J. L.; Kirchner, N. J., van Koppen, P. A. M.; Bowers, M. T. *J. Am. Chem. Soc.* **1989**, *111*, 2401.

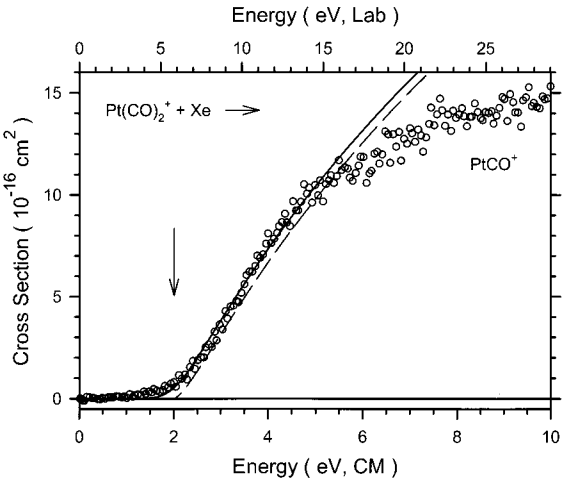

Figure 3. Zero pressure extrapolated cross sections for the reaction of $Pt(CO)_2^+$ with Xe as a function of kinetic energy in the center-of-mass frame (lower *x*-axis) and laboratory frame (upper *x*-axis) to form $PtCO^+$ (open circles). The dashed line is a model of the CID cross section that uses eq 1 with the parameters in Table 2 for 0 K reactants, and the solid line is the same model convoluted over the translational and rovibrational energy distributions of reactants. The vertical arrow indicates the 0 K threshold for loss of one CO ligand at 2.0 eV.

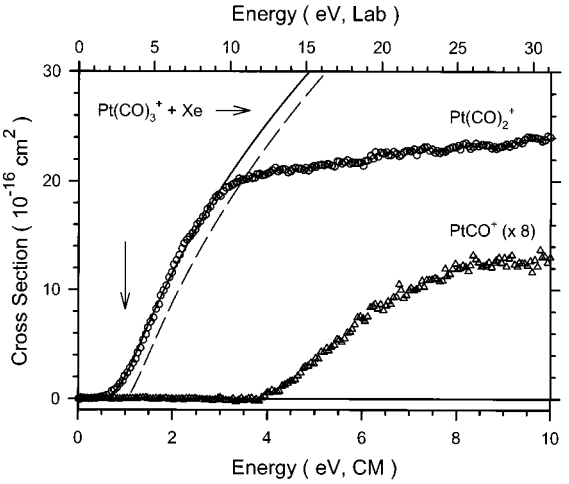

Figure 4. Zero pressure extrapolated cross sections for the reaction of $Pt(CO)_3^+$ with Xe as a function of kinetic energy in the center-of-mass frame (lower *x*-axis) and laboratory frame (upper *x*-axis) to form $Pt(CO)_2^+$ (open circles) and $PtCO^+$ (open triangles, multiplied by a factor of 8). The dashed line is a model of the cross sections of $Pt(CO)_2^+$ that uses eq 1 with the parameters in Table 2 for 0 K reactants, and the solid line is the same model convoluted over the translational and rovibrational energy distributions of reactants. The vertical arrow indicates the 0 K threshold for loss of one CO ligand at 1.02 eV.

the sequential loss of CO ligands because the total cross section remains fairly constant at elevated energies.

The magnitudes of the cross sections for reactions 2 increase with the number of CO ligands in the $Pt(CO)_x^+$ reactants. This reflects the larger size of the complex, the larger number of equivalent dissociation pathways, and the decreasing bond energies.

BDEs from Primary Thresholds. As concluded in our previous CID experiments, our best measurement of the bond dissociation energies for $M(CO)_x^+$ ions comes

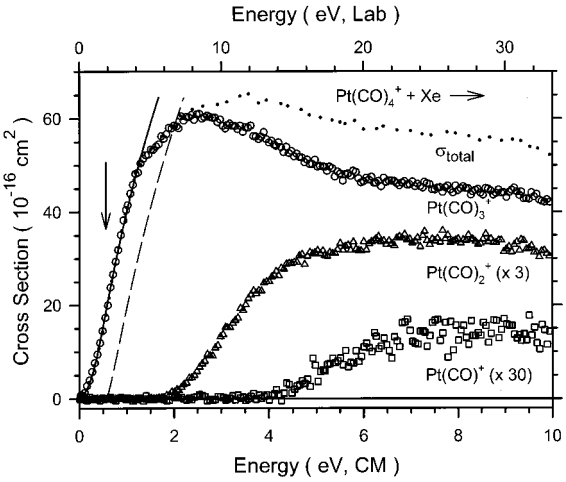

Figure 5. Zero pressure extrapolated cross sections for the reaction of $Pt(CO)_4^+$ with Xe as a function of kinetic energy in the center-of-mass frame (lower *x*-axis) and laboratory frame (upper *x*-axis) to form $Pt(CO)_3^+$ (open circles), $Pt(CO)_2^+$ (open triangles, multiplied by a factor of 3), and $PtCO^+$ (open squares, multiplied by a factor of 30). The total dissociation cross section for loss of CO ligands is indicated by the dotted line. The dashed line is a model of the cross sections of $Pt(CO)_3^+$ that uses eq 1 with the parameters in Table 2 for 0 K reactants, and the solid line is the same model convoluted over the translational and rovibrational energy distributions of reactants. The vertical arrow indicates the 0 K threshold for loss of one CO ligand at 0.55 eV.

Table 2. Summary of Parameters of Eq 1 for Modeling Primary CO Loss and Ligand Exchange Reactions

species	σ_0	n	E_0 (eV)
Pt^+-CO	1.5 ± 0.4	1.6 ± 0.1	2.20 ± 0.10
$(CO)Pt^+-CO$	9.4 ± 2.0	1.5 ± 0.1	2.00 ± 0.10
$(CO)_2Pt^+-CO$	18.1 ± 2.0	1.5 ± 0.1	1.02 ± 0.05
$(CO)_3Pt^+-CO$	66.6 ± 1.0	1.5 ± 0.1	0.55 ± 0.05
Pt^+-Xe	0.34 ± 0.15	2.5 ± 0.3	1.34 ± 0.30

from analysis of the primary dissociation channels, reactions 2. These are the least susceptible to the effects of kinetic shifts, competition with other channels, and multiple collisions. Listed in Table 2 are the optimized parameters of eq 1 obtained from the analyses of reactions 2 for the $Pt(CO)_x^+$ ($x = 1-4$) systems. These models are shown in Figures 2−5 and can be seen to reproduce the data well in the threshold regions. The σ_0 and E_0 values properly reflect the relative magnitudes and thresholds noted above.

Ligand-Exchange Reaction. Analysis of the cross section for the ligand exchange reaction 3 in the $PtCO^+$ system, Figure 2, leads to a threshold of 1.34 ± 0.30 eV (Table 2). The BDE of $PtXe^+$ can be determined from the difference between this threshold and the threshold measured for the reaction of $PtCO^+ + Xe$ to form $Pt^+ + CO + Xe$. This gives a value of $D_0(Pt^+-Xe)$ at 0.86 ± 0.30 eV, consistent with values derived from ligand exchange processes of other PtL^+ species.[41,60] This bond energy can be compared to other transition metal ion bond energies to Xe that range from 0.4 to 0.9 eV.[4,5,10,61−66]

One possible complication in the accurate determination of BDEs by CID experiments is whether ligand

(60) Zhang, X.-G.; Armentrout, P. B. Work in progress.

Table 3. Thresholds for Loss of Multiple Ligands (eV)

process	σ_0	n	E_0(calc)[a]	E_0(exp)[b]
$Pt(CO)_3^+ \rightarrow PtCO^+ + 2\ CO$	3.2 ± 0.1	1.0 ± 0.1	3.02 ± 0.10	4.42 ± 0.10
$Pt(CO)_4^+ \rightarrow PtCO^+ + 3\ CO$	1.2 ± 0.1	1.0 ± 0.1	3.57 ± 0.10	4.44 ± 0.15
$Pt(CO)_4^+ \rightarrow Pt(CO)_2 + 2\ CO$	14.1 ± 0.1	1.3 ± 0.1	1.57 ± 0.05	2.20 ± 0.10

[a] Thresholds calculated from the sum of primary thresholds listed in Table 2. [b] The optimized E_0 for these processes are obtained from analyses of zero-pressure extrapolated data sets.

exchange reactions, such as reaction 3, might cause a competitive shift in the observed threshold for the CID process, especially if the cross section for the ligand exchange process is large. This is a general problem for all CID processes because the ligand exchange process will always have a lower threshold than the CID process, no matter what neutral reagent is used. As discussed in detail elsewhere,[8,40] we do not believe that this competition is likely to affect our measurements here. First, the cross section for the ligand exchange reaction 3 declines rapidly once the CID product is formed (Figure 2). This is evidence for efficient energy transfer to the platinum carbonyl cation upon collision with Xe. Second, BDEs obtained from CID reactions in previous studies are generally in excellent agreement with theory and experiments for a number of different systems.[3−8,40,48,49] This demonstrates that competitive shifts are small or negligible.

BDEs from Secondary Thresholds. In principle, the difference in the thermodynamic thresholds for loss of successive CO ligands should yield thermochemical information. The difference between the thresholds for formation of $Pt(CO)_{x-2}^+$ and $Pt(CO)_{x-1}^+$ from CID of $Pt(CO)_x^+$ should be the same as the primary threshold for CID of $Pt(CO)_{x-1}^+$. However, secondary thresholds are generally higher than those calculated from the primary thresholds for metal carbonyl systems.[3−6,8] The poor agreement stems from the difficulties that (a) the probability for dissociation at the true thermodynamic threshold decreases as the extent of dissociation increases because the neutral products in the primary dissociation events can carry away energy, and (b) the higher thermodynamic thresholds for secondary dissociation lead to larger kinetic shifts. In addition, the effects of multiple collisions discussed above are enhanced for secondary processes and lead to appreciable corrections upon extrapolation to zero pressure (Figure 1). In the majority of cases[3−6,8] and here (Table 3), these systematic effects work in opposite directions but do not serve to cancel one another. For the loss of two CO ligands from $Pt(CO)_x^+$ (x = 3 and 4), the measured secondary thresholds are much higher than the thermodynamic values from the sum of the primary thresholds. Indeed, the threshold for the loss of three CO ligands from $Pt(CO)_4^+$ is comparable with that for the loss of two CO ligands from $Pt(CO)_3^+$, which cannot be correct. Overall, these results again demonstrate that the primary thresholds are our most accurate source of thermochemical information.[3−11]

Discussion

Attractive charge-induced dipole interactions between a metal ion (M^+) and neutral molecules/ligands (L) lead to association reactions with no barrier to produce ML_x^+ species.[58] If there is no change of electronic structure on M^+, the bond energies of ML_x^+ are expected to decrease monotonically with the number of ligands. This is a result of the declining effective charge on the metal as more ligands are attached and increasing repulsive interactions between ligands that become more sterically crowded. This is the situation found in alkali metal complexes because of the closed shell electronic structure for M^+.[10,67,68] However, transition metal systems are more complicated, and an understanding of metal−ligand bonding can require consideration of the loss of exchange energy, the energetic cost of promotion to the bonding state, sd hybridization, changes in spin states upon dissociation, ligand−ligand and metal−ligand repulsion, and π-back-bonding.[31,38,67−72]

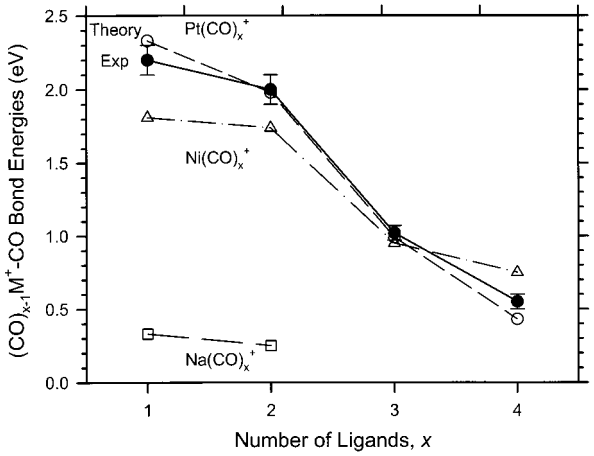

Figure 6. Bond energies for loss of one ligand from $Pt(CO)_x^+$ (open circles for theoretical values,[19] solid circles for experimental values), $Ni(CO)_x^+$ (open triangles),[7] and $Na(CO)_x^+$ (open squares)[10] as a function of the number of ligands. Error bars are indicated for the experimental BDEs of $Pt(CO)_x^+$.

Sequential BDEs of $Pt(CO)_x^+$. The ground electronic states of all four $Pt(CO)_x^+$ complexes have doublet spin,[19] as does Pt^+, such that all dissociation processes examined here are spin-allowed. Therefore, it is reasonable that the sequential BDEs of $Pt(CO)_x^+$ decrease monotonically with the number of CO ligands, Figure 6. However, the Pt^+−CO and $(CO)Pt^+$−CO BDEs are much stronger than those for $Pt(CO)_x^+$ (x = 3 and 4). This trend in sequential BDEs can be explained using sdσ hybridization.[3−10,31,38,67−69] The first CO ligand

(61) Haynes, C. L.; Armentrout, P. B.; Perry, J. K.; Goddard, W. A., III. *J. Phys. Chem.* **1995**, *99*, 6340.
(62) Haynes, C. L.; Armentrout, P. B. *Chem. Phys. Lett.* **1996**, *249*, 64.
(63) Haynes, C. L.; Fisher, E. R.; Armentrout, P. B. *J. Am. Chem. Soc.* **1996**, *118*, 3269.
(64) Sievers, M. R.; Armentrout, P. B. *J. Phys. Chem. A* **1998**, *102*, 10754.
(65) Tjelta, B. L.; Armentrout, P. B. *J. Phys. Chem. A* **1997**, *101*, 2064.
(66) Tjelta, B. L.; Walter, D.; Armentrout, P. B. *Int. J. Mass Spectrom.* **2001**, *204*, 7.
(67) Armentrout, P. B. *Acc. Chem. Res.* **1995**, *28*, 430.
(68) Rodgers, M. T.; Armentrout, P. B. *Mass Spectrom. Rev.* **2000**, *19*, 215.

induces hybridization of the empty 6s orbital on Pt^+-($^2D,5d^9$) with the singly occupied 5dσ orbital directed along the bonding axis. Because the ground state of Pt^+ is $^2D(5d^9)$, no promotion energy is needed for sdσ hybridization. This hybridization effectively removes electron density from the metal−ligand axis by placing the electron density in a sdσ hybrid orbital that is largely perpendicular to this axis. This allows a shorter bond length and an enhancement of the electrostatic interaction between Pt^+ and the CO ligand. Because of the symmetry of the sdσ hybrid orbitals, electron density is removed along the bonding axis on both sides of the metal. Thus, a second CO ligand located 180° from the first CO ligand can also bind strongly to Pt^+ while keeping ligand−ligand interactions to a minimum. Indeed, DFT calculations find that both $PtCO^+$ and $Pt(CO)_2^+$ are linear ($C_{\infty v}$ and $D_{\infty h}$ symmetry, respectively).[19] The Pt−C bond lengths in the dicarbonyl are longer (1.984 Å) than those in the monocarbonyl (1.861 Å), consistent with slightly weaker binding for the second ligand. This decrease in bond energy is presumably a consequence of repulsive dipolar interactions between the two ligands.

Because of the symmetry of sdσ hybrids, a third CO ligand cannot bind as strongly as the first two ligands. If hybridization is lost completely, then a trigonal planar geometry with C−Pt−C bond angles of 120° is expected. In contrast, DFT calculations find a distorted trigonal planar structure (C_{2v}) for $Pt(CO)_3^+$ in which the bond angles are 163.0°, 98.5°, and 98.5°.[19] The CO on the 2-fold axis has a slightly longer Pt−C bond length, 2.004 vs 1.998 Å. Thus, some of the sdσ hybridization is retained. In analogy with similar situations calculated for $Co(H_2)_3^+$ [73] and $Co(CH_4)_3^+$,[61] it seems likely that some 6p character is probably introduced to polarize the occupied sdσ hybrid away from the third ligand. This costs more energy than sdσ hybridization and therefore is not as effective, such that the third ligand is bound much more weakly than the first two.

Calculations indicate that $Pt(CO)_4^+$ has D_{2d} symmetry with four equal Pt−C bond lengths of 2.030 Å and C−Pt−C bond angles of 153.3° for carbonyls in the same dihedral plane.[19] Thus, the molecule is a square planar complex that has distorted toward a tetrahedral geometry, presumably in order to avoid having the ligands point directly at the $d_{x^2-y^2}$ orbital that is singly occupied in this $5d^9$ complex. The fourth bond is probably weaker than the third because of larger steric repulsion between the CO ligands and because polarization of the sdσ hybrid orbitals no longer provides any energetic benefit. In this respect, it is interesting to note that the geometry of the $Pt(CO)_3^+$ complex can be understood in terms of a square planar complex that has lost one ligand and allowed the remaining ligands to distort toward the open site. It should also be pointed out that the geometry of the $Pt(CO)_x^+$ complexes must also be influenced by dπ−π* back-bonding interactions, but these cannot be assessed given the available information.

Table 4. Bond Energies of $Pt(CO)_x^+$ (eV)

	D_e(theory)[a]	D_0(theory)	D_0(exp)
Pt^+−CO	2.83[b]	2.33[c]	2.20 ± 0.10
$(CO)Pt^+$−CO	2.08	1.99	2.00 ± 0.10
$(CO)_2Pt^+$−CO	1.05	0.99	1.02 ± 0.05
$(CO)_3Pt^+$−CO	0.49	0.42	0.55 ± 0.05

[a] Reference 19. [b] Reference 57. [c] Spin−orbit correction to $^2D_{5/2}$ is made. See the text and refs 41 and 74.

Comparison with Calculated BDEs. No previous experimental results are available in the literature for comparison with the present results on the platinum carbonyl cation systems. However, comparisons can be made with DFT calculations.[19] The bond energies of $(CO)_{x-1}Pt^+$−CO calculated by Liang et al. were reported as D_e values.[19] To compare to the present experimental results, we adjust these values for zero-point energy corrections calculated using the vibrational frequencies of $Pt(CO)_x^+$ (Table 1). In addition, the DFT calculations do not explicitly include spin−orbit interactions, so that calculations involving dissociation to Pt^+ are referenced to the weighted average energy of the spin−orbit components of the ^2D term, 0.418 eV.[41,74] To properly compare to experimental values, which are referenced to the energy of the $^2D_{5/2}$ ground state at 0.0 eV, the calculated value must be corrected for this different asymptotic energy. The various theoretical values, as corrected here to D_0, are listed in Table 4. The theoretical BDEs are in good agreement with our experimental BDEs for all four complexes, as shown in Figure 6, and show the same qualitative trends. The differences (0.01−0.13 eV) between the theoretical and experimental values are comparable to the uncertainties.

Comparison with the First-Row Congener, $Ni(CO)_x^+$. Like the $Pt(CO)_x^+$ system, sequential BDEs for $Ni(CO)_x^+$ ions decline monotonically, and the first and second CO ligands are bound much more strongly than the third and fourth, Figure 6.[7] This trend is easily rationalized because Ni^+ has a $^2D(3d^9)$ ground state similar to the $^2D(5d^9)$ ground state of Pt^+, and the ground electronic states of $Ni(CO)_x^+$ ($x = 1-4$) have been calculated to have doublet spin.[19] Thus, no spin changes are required as CO molecules are successively added to Ni^+ to form $Ni(CO)_x^+$, as for $Pt(CO)_x^+$ systems.[19] In the nickel system, 4s−3dσ hybridization is responsible for the strong bonding between Ni^+ and the first and second CO ligands.[7]

DFT calculations indicate that the Pt^+−CO bond length is shorter than that for Ni^+−CO by 0.035 Å.[19] This is interesting given that Ni^+ is certainly smaller than Pt^+: covalent radii are 1.15 vs 1.29 Å, respectively, and the radii of the doubly charged cations are 0.72 vs 1.06 Å, respectively.[75] We attribute this difference in bond lengths to the lanthanide contraction and relativistic effects, which make the 6s orbital close in size to the 5d orbitals.[76−78] This leads to more efficient sdσ

(69) Barnes, L. A.; Rosi, M.; Bauschlicher, C. W., Jr. *J. Chem. Phys.* **1990**, *93*, 609.
(70) Bauschlicher, C. W.; Langhoff, S. R.; Partridge, H. *J. Chem. Phys.* **1991**, *94*, 2068.
(71) Langhoff, S. R.; Bauschlicher, C. W.; Partridge, H.; Sodupe, M. *J. Phys. Chem.* **1991**, *95*, 10677.
(72) Walter, D.; Armentrout, P. B. *J. Am. Chem. Soc.* **1998**, *120*, 3176.
(73) Bauschlicher, C. W., Jr.; Maitre, P. J. *J. Phys. Chem.* **1995**, *99*, 3444.
(74) Moore, C. E. *Atomic Energy Levels*, NSRDS-NBS; 1971; 35/Vol. III.
(75) Wilson, R. G.; Brewer, G. R. *Ion Beams with Applications to Ion Implantation*; Wiley: New York, 1973.
(76) Ohanessian, G.; Brusich, M. J.; Goddard, W. A., III. *J. Am. Chem. Soc.* **1990**, *112*, 7179.
(77) Irikura, K. K.; Beauchamp, J. L. *J. Phys. Chem.* **1991**, *95*, 8344.

hybridization for the platinum system and thereby a stronger electrostatic interaction between Pt^+ and the CO ligand. In contrast, the $(CO)_{x-1}Pt^+-CO$ bond lengths for $x = 2-4$ are calculated to be longer than those for $(CO)_{x-1}Ni^+-CO$ by 0.043−0.053 Å, more consistent with the relative sizes of the central atomic ions; however, the bond energies in the platinum system do not become less than those in the analogous nickel complexes until $x = 4$, Figure 6. This is again consistent with more efficient sdσ hybridization for $Pt(CO)_x^+$ ($x = 1-3$).

Comparison with Sodium Carbonyls. Alkali metal ions have a spherically symmetric closed shell electronic structure. In alkali metal carbonyl cations, no change of electronic structure is energetically accessible for the central metal ion. Therefore, bonding is found to be totally electrostatic,[10] such that the sequential BDEs gradually decrease with increased ligation. The radius of Pt^+ has not been characterized but should be about 1.2 Å, the mean of the covalent radius, 1.3 Å, and the +2 cation radius of 1.06 Å.[75] This radius is larger than that of Na^+ (0.98 Å);[75] however, BDEs of platinum mono- and dicarbonyl cations are about seven times stronger than those of the corresponding sodium carbonyl cations (0.33 ± 0.08 and 0.25 ± 0.03 eV)[10] (Figure 6). This shows that the bonding cannot be totally electrostatic for platinum mono- and dicarbonyl cations. As discussed above, part of this large enhancement can be attributed to favorable sdσ hybridization, but contributions from covalent σ-donor and π-back-bonding are also operative in the platinum carbonyl cations.[10] As noted above, the effects of sdσ hybridization have been lost almost completely for $Pt(CO)_4^+$. Nevertheless, the $(CO)_3Pt^+-CO$ bond energy is still larger than the electrostatic $Na(CO)_x^+$ bond energies. This is an indication that covalent σ-donor and π-back-bonding interactions remain in the $Pt(CO)_4^+$ complex, as also concluded above.

(78) Irikura, K. K.; Goddard, W. A., III. *J. Am. Chem. Soc.* **1994**, *116*, 8733.

Conclusion

We report systematic measurements of the collision-induced dissociation of $Pt(CO)_x^+$ ($x = 1-4$) ions with Xe using guided ion beam tandem mass spectrometry. From the thresholds for these processes and a ligand exchange reaction, bond dissociation energies at 0 K are determined for Pt^+-CO, $(CO)Pt^+-CO$, $(CO)_2Pt^+-CO$, $(CO)_3Pt^+-CO$, and Pt^+-Xe (Tables 2 and 4). The trends in the sequential bond energies of $Pt(CO)_x^+$ ($x = 1-4$) are discussed and compared with theoretical values, isovalent $Ni(CO)_x^+$ systems, and spherically symmetric closed shell $Na(CO)_x^+$ systems. The trends in sequential BDEs are explained in terms of sdσ hybridization at the central metal ion, electrostatic interactions, and ligand−ligand steric interactions. Larger bond energies for platinum carbonyl cations (especially, $x = 1$ and 2) vs nickel ones are attributed to more efficient sdσ hybridization, a consequence of the lanthanide contraction and relativistic effects. A comparison of BDEs of platinum carbonyl ions to those of sodium carbonyl ions illustrates that sdσ hybridization and covalent interactions greatly enhance the metal binding to CO ligands.

Acknowledgment. This work was supported by the National Science Foundation under Grant CHE-9877162. X.-G.Z. thanks Drs. Rohana Liyanage, Jay Amicangelo, and Karl Irikura for informative discussion. The authors thank B. Liang and L. Andrews for providing additional computational results from their work.

OM010390D